Breaking Down the Delta Wing Vortex

The Role Of Vorticity in the Breakdown Process

R. C. Nelson and K. D. Visser

Department of Aerospace and Mechanical Engineering
University of Notre Dame
Notre Dame, Indiana 46556
USA

AGARD Symposium on Vortex Flow Aerodynamics

October 1-4, 1990 Scheveningen, The Netherlands

Breaking Down The Delta Wing Vortex

The Role of Vorticity in the Breakdown Process

R. C. Nelson and K. D. Visser

Department of Aerospace and Mechanical Engineering
University of Notre Dame
Notre Dame, Indiana 46556
The United States of America

Abstract

Experimental x-wire measurements of the flowfield above a 70° and 75° flat plate delta wing were performed at a Reynolds number of 250,000. Grids were taken normal to the wing at various chordwise locations for angles of attack of 20° and 30°. Axial and azimuthal vorticity distributions were derived from the velocity fields. The dependence of circulation on distance from the vortex core and on chordwise location was also examined. The effects of nondimensionalization in comparison with other experimental data is made. The results indicate that the circulation distribution scales with the local semispan and grows in a nearly linear fashion in the chordwise direction. The spanwise distribution of axial vorticity is severely altered through the breakdown region and the amount of vorticity present appears to reach a maximum immediately preceding breakdown. The axial vorticity components with a negative sense, such as that found in the secondary vortex, seem to remain unaffected by changes in wing sweep or angle of attack, in direct contrast to the positive components. In addition, the inclusion of the local wing geometry into a previously derived correlation parameter allows the circulation of growing leading edge vortex flows to be reduced into a single curve.

Nomenclature

c	chord
r	radial direction
r_c	vortex core radius
P	pressure
Re	Reynolds number
s	semi span
s*	local semi span
U_∞	freestream velocity
V_i	velocity in the i direction
x	chordwise direction
y	spanwise direction
z	direction normal to wing surface
α	angle of attack
ε	apex half angle
Γ	circulation
Λ	sweep angle
ϕ	angular direction
Ω_i	vorticity in the i direction

Introduction

The underlying physics of the vortex structure above a delta wing planform, and more particularly the process by which the flowfield undergoes the rapid transition referred to as vortex breakdown, has been a topic of concern for many years in the aerospace field. At high angles of attack, the boundary layer on the lower surface of the delta wing flows outboard. The fluid separates at the sharp leading edge, forming a free shear layer which curves upward and rolls into a core of high vorticity on the top side of the wing. Each of the two counter-rotating vortices also contain axial flow components in the central core regions, around and along which the fluid spirals. This axial flow can attain velocities up to three times the freestream value.

Additional spanwise outflow is induced on the upper surface beneath the coiled vortex sheet. The fluid separates from the surface as it approaches the leading edge to form the so called "secondary vortices". The main effect of the secondary vortex is to displace the primary vortex upwards and inwards. The size and strength of the primary vortex increases with angle of incidence. It becomes the dominant steady flow feature through a wide range of practical flight attitudes. The acceleration of the flow in these vortices results in an incremental lift termed the "vortex" or "nonlinear" lift. As much as 30% of the total wing lift is attributable to the pressure distribution created on the wing surface by these leading edge vortices.

Delta wing performance is limited, however, by a phenomenon known as vortex breakdown. Breakdown, or "bursting" as it is sometimes referred to, is characterized by an increase in vortex diameter followed by large scale turbulent dissipation and a decrease in the core's axial and circumferential velocity. This leads to a loss of lift and a reduction in the magnitude of the nose down pitching moment. Experimental, theoretical, and numerical investigations have been carried out in an effort to not only understand what is occurring, but to predict the onset of this drastic change in the flowfield. Efforts have included variation of all manner of possible parameters, including wing geometry, angle of attack, and Reynolds numbers.

Most investigators approach the study of delta wing vortical flows, however, by asking such questions as: "Why does vortex breakdown occur?" and "What factors influence breakdown?" A different perspective on the problem can be gained by posing the inverse question: "Why does the vortex manage to maintain a cohesive flow structure upstream of the transition/breakdown region?" In other words, with core velocities measured at over three times that of the freestream velocity and corresponding circumferential velocities approaching 2.5 times of freestream: "Why does it stay together for as long as it does, instead of breaking down immediately?" This was the motivation for the current investigation.

Background

Many factors can influence vortex breakdown. Lambourne and Bryer [1] suggest the total pressure in the core and the adverse pressure gradient along the axis are essential factors in causing breakdown to occur. Harvey [2] observed that variation of the swirl of the flow in tube vortices indicated breakdown to be an intermediate stage between two types of flow: those that exhibit axial velocity reversal and those that do not.

Erickson [3] discusses in detail the effect of Reynolds number on vortex flow development. From experiments it appears that large scale vortex structures are determined primarily by convective transport mechanisms, implying an independence of Reynolds number. Erickson concludes that the majority of the phenomena observed in the delta wing flow field is dominated by potential flow effects associated with the external field, ie. the pressure gradient.

An extensive literature review by Payne [4] on the factors which can influence breakdown is summarized below. Increasing the sweep angle or decreasing the angle of attack causes the location of the breakdown to move aft. The breakdown position will move forward during flow acceleration and remain so until the steady speed condition is reached whereupon it returns to its normal breakdown position [1]. The reverse is true for deceleration. The actual position of this breakdown is a strong function of the pressure gradient along the vortex, the initial axial core velocity, and the angle of sideslip, or yaw angle. An increase in the swirl of the flow or a larger adverse pressure gradient tends to promote the onset of breakdown.Thicker wings, rounded leading edges, lower Reynolds numbers, and of course more complex geometries can also substantially influenced the location of breakdown. Kegelman and Roos [5] investigated leading edge geometries, ranging from blunt rounded edges to leeward and windward bevels, and found the breakdown location to be strongly affected by these geometric variations. In addition, the maximum value of the lift curve was found to be significantly affected by this variation in leading edge shape.

Payne has also listed factors examined by other investigators in the literature which have been found to have little or no influence on the breakdown position. Effects due to changes in the Reynolds number are small at high Reynolds numbers. This applies to sharp edged, thin delta wings at moderate angles of attack. The breakdown position seems to be independent of the turbulent breakdown of the shear layer near the leading edge. Attempts at altering the leading edge by Lambourne and Bryer [1], including a trip wire on the upper surface had no significant effect. Wentz [6] observed that variation of the trailing edge geometry of 70° sweep delta, diamond and arrow planforms, had a negligible effect on vortex breakdown location. Wentz also found [7] that the vortex breakdown region crossed the trailing edge at the same angle of attack for all these trailing edge configurations.

The complexities of this vortical flow are such that a complete analytical solution is difficult to obtain. Theories do exist that partially predict the occurrence of certain flow phenomena, such as vortex breakdown in which the vortex behavior changes dramatically, and to indicate the sensitivity of the breakdown region to the severity of axial pressure gradients. Several pertinent breakdown theories are summarized below, and a more extensive discussion can be found in Wedemeyer [8]:

Ludweig [9] has suggested that the spiral form of breakdown results from hydrodynamic instabilities in the flow due to upstream spiral disturbances. A similar view of breakdown was developed by Jones [10].It has been proposed by Squire [11] that breakdown is a standing wave phenomenon. Once the flow is capable of supporting infinitesimal standing waves, downstream disturbances can propagate upstream and therefore disrupt the flow. Randall & Leibovich [12] contend that this is in fact a finite amplitude wave.

Another hypothesis is the view taken by Benjamin [13]. He suggests that breakdown is a finite transition (subcritical to supercritical) between conjugate flow states analogous to the hydraulic jump in open channel flows. While Squire postulated that the existence of waves leads to breakdown, Benjamin claims that the leading wave is the breakdown. Escudier [14] goes a step further by proposing a two stage (supercritical-supercritical supercritical-subcritical) transition. The first stage is isentropic while the latter is not. In addition, his analysis suggests breakdown occurs for a unique swirl number $\Gamma / \pi r_c U_\infty$ which is equal to 1.414 for a Rankine vortex with an infinitesimally small core radius, r_c. In a theory analogous to boundary layer separation, Gartshore [15] concluded that breakdown occurred because of a diffusion of vorticity from the core of the vortex.

Several theories rely on the supposition that breakdown is predicted by the failure of the quasicylindrical approximations of the equations of motion. Hall [16], in 1966, suggested that breakdown is associated with some change in the flowfield outside the core, such as the rate of feeding of vorticity or the pressure. Bossel [17] used the ideas of Hall to estimate that a swirl angle, defined as $\tan^{-1}(V_Z / V_X)$,

of 54.8° anywhere in the vortex would cause flow stagnation. Mager [18] associated a singularity in the incompressible quasicylindrical momentum-integral solution with breakdown. Wilson [19] approached the problem in a similar manner to obtain a swirl parameter for thin delta wings in subsonic flow.

Grabowski and Berger [20], using solutions of the full, steady, axisymmetric Navier-Stokes equations, concurred with Hall [21] in that breakdown is the result of a critical retardation of the flow. As well, his results also showed that a vortex with sufficient swirl can be reduced to the critical breakdown state by diffusion of vorticity, flow divergence and pressure forces.

A recent hypothesis has been proposed by Brown and Lopez [22] on the physical mechanism governing vortex breakdown which occurs in confined cylindrical flows. Variation of the problem parameters has resulted in an axial flow deceleration great enough to sustain a stagnant flow region containing recirculating fluid. This phenomena is very similar to that seen in cylindrical tubes and over delta wings. Their basic argument is that the physical mechanisms involved in the breakdown process rely on the production of negative azimuthal vorticity, that is

$$\Omega_\phi = \frac{\partial V_r}{\partial x} - \frac{\partial V_x}{\partial r}$$

which results from a tilting and stretching of the predominantly axial vorticity vector as seen in Figure 1. They then address the question of why the strong vortical core diverges by considering the Euler equation of the radial momentum and comment on how this type of mechanism would apply to a delta wing flowfield. Their analysis eventually leads to the following inequality

$$\frac{V_\phi^2}{r} - \frac{1}{\rho}\frac{\partial P}{\partial r} > 0$$

which would then initiate breakdown. Brown and Lopez hypothesize that vorticity diffusion leads to a radial redistribution of the circulation and a stretching and tilting of vortex lines due to a local increase of the tangential velocity, V_ϕ. This is followed by a reduction in the initially positive azimuthal component of vorticity with axial distance and the subsequent beginning of an 'inviscid breakdown' process.

As of yet, none of these ideas are sufficient to accurately predict vortex breakdown. Recent work by O'Neil, Barnett, and Louie [23] and Ekaterinaris and Schiff [24] using Euler and Navier-Stokes codes respectively have demonstrated a vortex breakdown in their results for certain conditions. These computational results do correspond to experimental data. However, no theory exists which can yield the flow detail in the breakdown zone nor universally predict breakdown locations which consistently compare with experimental results. Because of this, it is essential that the flowfield be examined

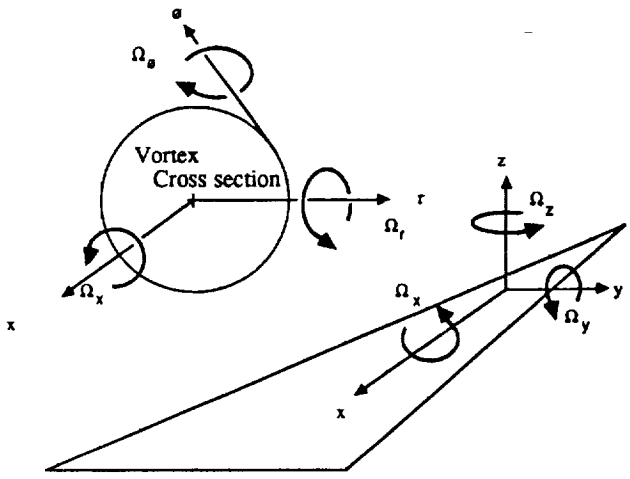

Figure 1. Delta Wing Vortex Geometry

experimentally in an effort to uncover information which may shed light on this problem.

The vortex flowfield can be regarded as a transition from one flow state to another which may occur as a result of a combination of certain flow parameters reaching a critical or unstable state. One can attempt to quantify such critical breakdown parameters in two forms: as a function of either the independent or the dependent variables. The former would involve factors such as angle of attack, sweep angle of the wing, and sideslip. An indication parameter involving dependent variables would be based upon flow conditions which result from the geometry of the problem. Items such as local vorticity and chordwise pressure gradient fall into this category.

The determination of such breakdown indication parameters could be based on several forms:

a. A local balance between the generation and convection of vorticity.
b. A local balance of the pressure forces with the acceleration of the fluid.
c. The size of the local length scale compared to the wing geometry.
d. An empirical fit parameter based on wing geometry, angle of attack, etc.

The aspects of the vorticity field would seem to be of utmost importance in gaining a better understanding of the flowfield behavior. Both the generation of vorticity, which is transported into the vortex, and the convection rate downstream of this vorticity could play a crucial role in determining where the breakdown of the primary vortex occurs as suggested by Lee and Ho [25]. The complete role of the secondary vortex, which is a direct result of the viscous nature of the flow, is also not well understood. Its presence, illustrated in Figure 2 via a titanium tetrachloride vapor method for marking vortical flows [26], is known to displace the primary vortex inwards and upwards. Questions still remain, however, as to the effect of the secondary vortices on the reduction of the primary vortex pressure peaks as compared to an Euler type solution, or on even more nebulous concepts such as the effect on the vorticity distribution above the wing surface.

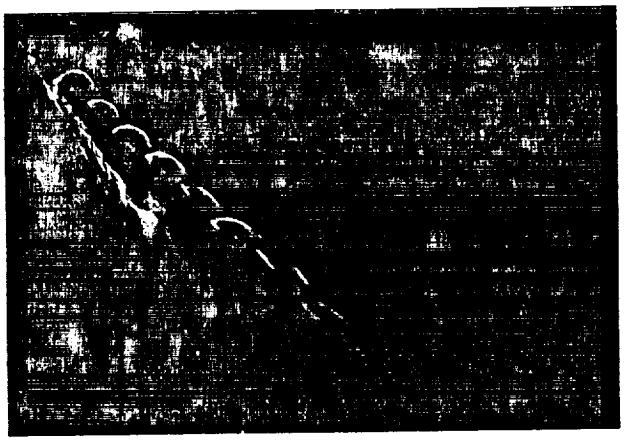

a)

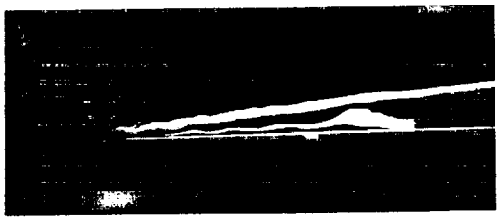

b)

Figure 2. Flow Visualization of Primary and Secondary Vorticies a) three quarter view, b) side view

Although the data base of delta wing flowfield information is growing, most experimenters are constrained to a specific configuration at a fixed angle of attack or chord location. This information, helpful for the sake of comparison, provides little or no information on the changing flow field state in the chordwise direction. Aspects such as rate of vorticity generation or circulation distribution in the streamwise direction are impossible to address.

In addition, there are other subtler reasons which make comparison difficult. Data compiled from several different investigators [27 - 30] is compared in Table 1. Both the sweep angles and the angles of attack are roughly the same. The values of vorticity presented are the maximum values found in the flow field and coincide with the core axis. Typically, investigators use the model chord, c, and the freestream velocity, U_∞, as nondimensionalizing scales for the flow. The results are seen to vary quite substantially. The local semispan, s* could also be considered a viable length scale, since flow visualization indicates the vortex structures to scale with the wing geometry. Use of the local semispan would account for local geometric changes due to sweep angle and allow for comparison of data taken at different chord stations. The data of Kjelgaard and Sellers [27], for example, indicates a lower value of vorticity than that of Payne for a location 20% farther from the apex. If s* is used as a scaling factor, the magnitude of the axial vorticity component is seen to exceed that of Payne. It is also noted that identical geometries, such as that of Payne and the current investigation, have produced different values of the axial vorticity component. These differences indicate there are other factors which have not been taken into account. A closer examination of the grid resolution of each investigation provides some insight. As indicated in Table 1, the highest derived vorticity values correspond to the finest grid resolution and vice versa. Since vorticity is a measure of the smallest scales of the flow, it would only make sense that a finer measurement grid would be able to 'capture' the high gradients of velocity present in the field. These differences in flowfield measurement add to the difficulty in obtaining a clear picture of the physics involved.

Table 1. Maximum Axial Vorticity Data

Investigator	Angle of Attack (°)	Sweep Angle (°)	Chord (mm)	Freestream Velocity U_∞ (m/s)	Chordwise Station x/c	Maximum Vorticity Ω_x (1/s)	$\frac{\Omega_x c}{U_\infty}$	$\frac{\Omega_x s^*}{U_\infty}$	Measurement Grid Resolution (y/s)
Payne	20.0	75	406.4	10	0.5	8,383	341	46	0.04166
Kjelgaard and Sellers	20.5	75	568.8	12.8	0.7	7,113	316	59	0.0323
Visser and Nelson	20.0	75	406.4	9.7	0.5	12,340	517	69	0.030
	20.0	75	406.4	10.0	0.5	22,774	925	124	0.015
Verhaagen	20.4	76	2220.0	25	0.5	17,400	1545	193	0.0145
Carcaillet	20.0	75	500	20.3	0.6	23,061	568	91	•
	20.0	75	500	119	0.6	114,144	480	77	•
	20.0	75	1450	40	0.8	11,034	400	86	•
Pagan and Solignac	19.3	75	560	14.5	1.4 (wake)	6,732	260	70	•

For the reasons stated above, a study was undertaken to measure the delta wing flowfield at various chordwise locations over delta wings. Models with different sweep angles at different angles of attack were used in an attempt to determine if the flow reaches some measurable critical state, particularly involving aspects of the vorticity components, that would then initiate a flow transition to the post breakdown state.

Experimental procedures

All experiments were carried out in the University of Notre Dame subsonic wind tunnel facilities. The tunnel is powered by an 18.6 kw AC induction motor which drives an 8 bladed 1.2 meter (4 foot) fan located in the diffuser outlet (Figure 3). The four degree of freedom, computer controlled, probe traversing test section is preceded by a 24:1 contraction inlet. The minimum step sizes possible in the streamwise, spanwise, and normal directions were 0.0064mm, 0.0254mm, and 0.0208 mm respectively. The section dimensions were 610 mm by 610 mm by 1820 mm (24 by 24 by 76 inch). The models used were flat plate delta wings having a windward 25° bevelled edge, a root chord of 406.4 mm (16 inches) and a thickness of 6.35 mm (0.25 inches). The minimum distance between the wing surface and the probe was 3.0 mm due to probe geometry.

A TSI IFA 100 constant temperature annemometer system was used to acquire the data in conjunction with a Macintosh II computer which also maneuvered

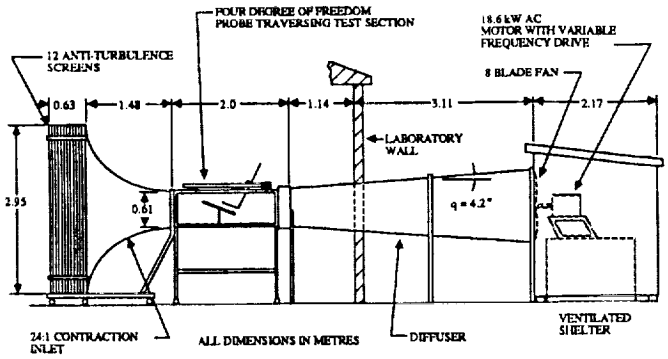

Figure 3. Notre Dame Subsonic Wind Tunnel Facility

the x-wire probe in the test section. The probes utilized five micrometer diameter tungsten wires giving an length/diameter ratio of 250. Overheat ratios were set to 1.8. The wires were calibrated for every test to reduce the possible errors associated with property changes of the wires. In addition, this procedure eliminated the need for temperature compensation as the ambient temperature did not vary by more than ± 1° C over the course of any individual test.

The technique of Sherif and Pletcher [31] was employed to determine the magnitudes of the velocity components.This is based on the effective velocity measurement method. The wire senses a velocity composed of vectors normal and tangential to the wire which cool the wire at different rates, k_1 and k_2. Jørgensen [32] has expressed the most general form of this equation as:

$$U_{eff}^2 = U_N^2 + k_1^2 U_T^2 + k_2^2 U_B^2$$

for an X-wire lying in the NT plane (Figure 4a). The effective velocities were obtained using a least squares fit based on the calibration and then the method of Sherif and Pletcher [31] to determine the magnitudes of the velocity components.

In order to fully determine the three velocity components and their associated directions, however, it was necessary to take four normal grid sweeps above the wing at each chordwise location. Two x-wire probe configurations were utilized and are shown in Figure 4b. Probe 1, a DISA 55P62, had wires lying in a plane perpendicular to the probe axis, while the wires of probe 2, a DISA 55P61, were lying in a plane parallel to the probe axis, as shown by the accompanying schematic. The initial two grid sweeps used probe 1 with wire 1 at the reference of zero degrees and wire 2 at negative 90 degrees using the geometry in Figure 4b and in accordance with that of Sherif and Pletcher [31]. The probe was then rotated 45° about its axis and a second sweep initiated.This provided enough information for the velocity magnitudes to be determined. The second probe was used to take two sweeps with the plane of the wires parallel to the wing and perpendicular to it respectively. This second set of sweeps determined the direction of the transverse (v) and normal (w) velocity components. It was assumed that the direction of u was always in the positive direction as the probe was kept in the flow forward of the breakdown region.

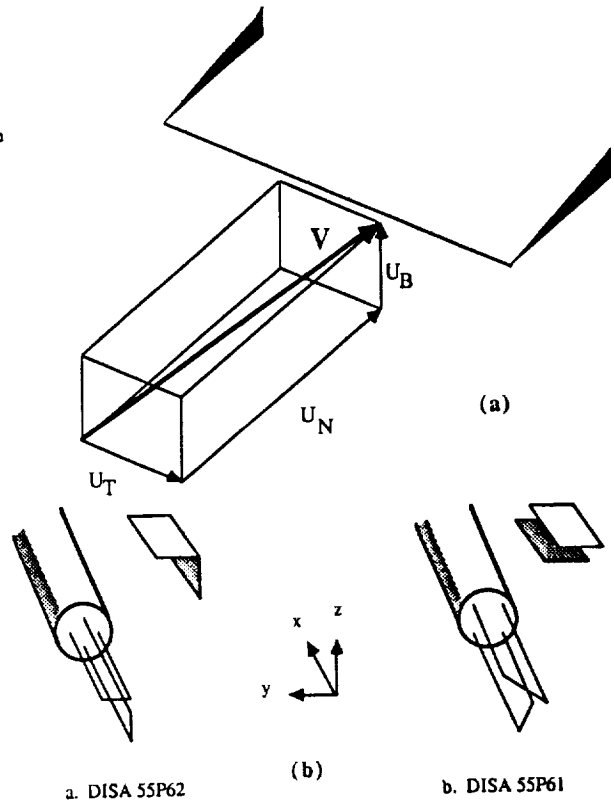

Figure 4. Hot Wire Probe Geometries and Configuration
a)Effective Velocity Coordinates of Jørgenson,
b) X-wire probes

Results and Discussion

The majority of data was accumulated over a 75° sweep delta wing at 20° angle of attack. Measurements were made at various chordwise stations in grid planes normal to the upper surface. The angle of attack was then increased to 30° and chordwise stations were measured upstream of the probe induced breakdown of approximately x/c = 0.5. Experiments by Payne, Ng, and Nelson [33] comparing LDV and seven hole probe data have shown that the effect of introducing a probe into the flowfield does not greatly distort the flowfield provided the measurements are taken upstream of the breakdown zone. Finally, a 70° sweep configuration was utilized at 20° angle of attack in an effort to observe the effect of sweep. All tests were conducted at a Reynolds number of 250,000.

Typical flowfield distributions are shown in Figure 5. The axial velocity u/U_∞ is actually the velocity normal to the measurement plane at the chordwise station. The jetting core structure of the vortex is seen to be quite well defined, with the majority of the measured field maintaining a velocity above the freestream velocity. Measurements encompassed a z/s of 0 to approximately 1 and were taken from the chord centerline out to a y/s of 1.2 on the right side of the wing. Using this grid, the details of the primary, secondary, and the shear layer can be captured. Grid increments were set to a y/s and z/s of 0.03 at each station. The transverse and normal

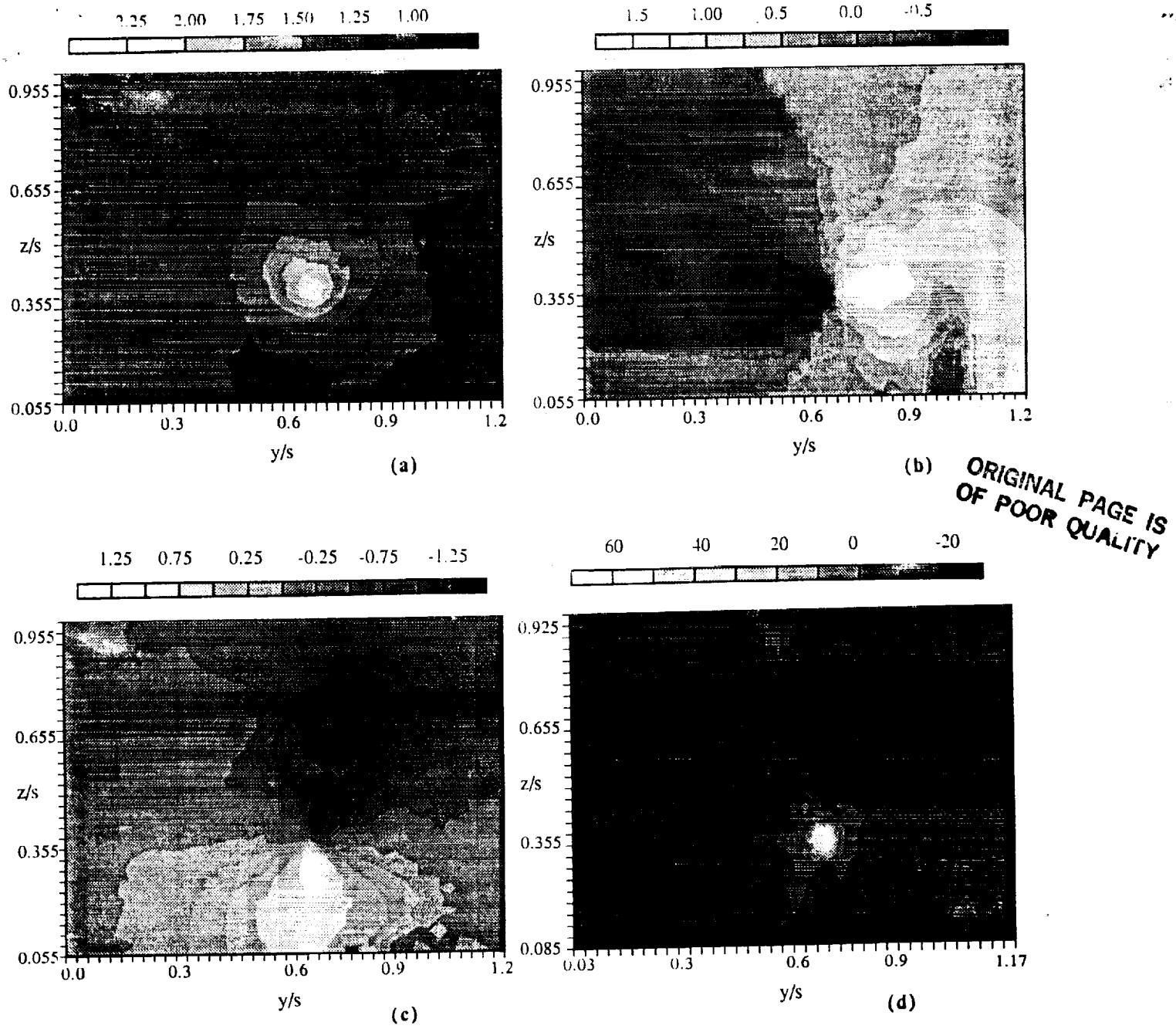

Figure 5. Chord Station Flowfield Maps for Sweep = 75°, Angle of Attack = 20°, x/c = 0.50
a) u/U_∞, b) v/U_∞, c) w/U_∞, d) Ωx

velocity components, v/U_∞ and w/U_∞ respectively, are depicted in Figures 5b and 5c. These data were then centrally differenced spatially to obtain the axial vorticity component,

$$\Omega_x = \frac{\partial w}{\partial y} - \frac{\partial v}{\partial z}$$

shown in Figure 5d.

Since the role of vorticity, including the effects incurred by the secondary vortex on the primary, was the motivation for this investigation, the local magnitudes and chordwise distributions were the logical places to begin. An initial proposition was that the vortex structure may be unable to exist in the cohesive, pre-breakdown nature if a maximum local value of vorticity in the vortex, say Ωx_{max}, is reached. Conventionally, investigators such as Kjelgaard and Sellers [27] have multiplied the calculated vorticity by the ratio of the root chord to the freestream velocity providing an overall view of the absolute vorticity in the entire flowfield. As mentioned previously, the use of the local spanwise distance provides a means to scale each crossectional flow plane in order to examine the effect of the local geometry on the flow characteristics. The local semispan was used to scale the current data in addition to using the chord.

The maximum value of vorticity was obtained at each station as well as the minimum. These values are presented in Figure 6 for the 75° sweep wing at 20° and 30° angle of attack. The vorticity data is nondimensionalized using the two conventions mentioned above. From Figure 6a, in which the

vorticity is multiplied by the ratio of the root chord to the freestream velocity, it appears that the magnitudes of both the positive and negative maximum values are decreasing with increasing distance from the apex. No breakdown existed over the wing for the 20° angle of attack case. The 30° case was seen to have a breakdown occurring between the 0.50 and 0.55 x/c location. The positive values of vorticity show a slight drop at this station, however the negative values show no change at all.

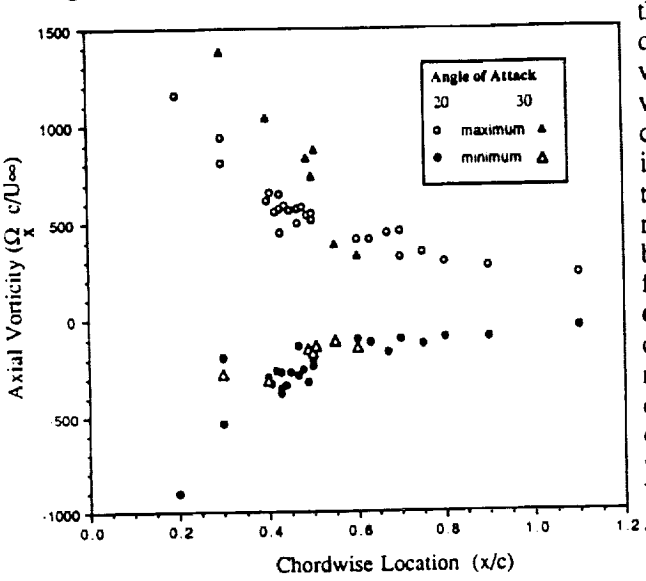

(a)

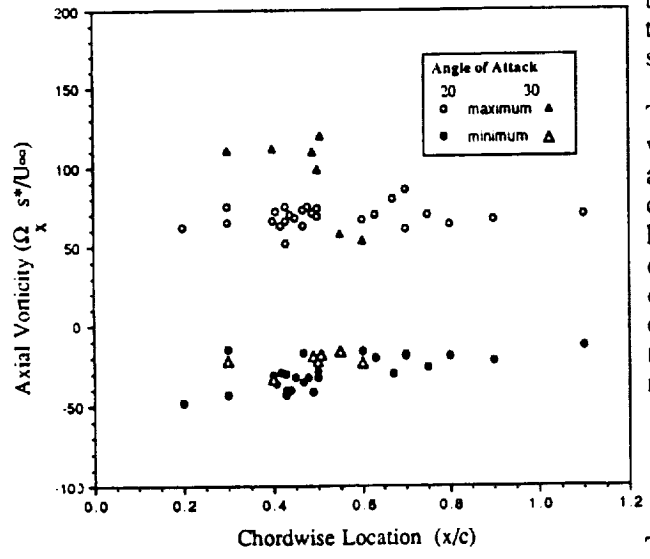

(b)

Figure 6. Chordwise Comparison of Maximum and Minimum Vorticity for 75° Sweep Nondimensionalized Using a) chord, b) local semispan

If the vorticity is now nondimensionalized by the local semispan, s*, as shown in Figure 6b, the data appears to indicate a constant value in the chordwise direction for both the positive and negative values. The drop in the positive value for the 30° case is more evident, however a large scatter in the data is still seen to exist.

This scatter in the data can be attributed to several factors. The vorticity is a measure of the smallest scales of the flow. Details of the velocity gradients will be lost if the grid is not sufficiently fine. In addition, these values of vorticity were obtained by differentiating discrete data which has the effect of increasing the error associated with such measurements. Therefore simply examining the maximum value of the vorticity is not enough to make a definitive statement of the vortex status at that chord station.

The leading edge sheet continually feeds vorticity into the vortex flowfield along the entire length of the delta wing. An interesting possibility is that the vortex can only 'hold' or contain a certain amount of vorticity before it must revert to a more stable configuration in order to contain or transport this increase in vorticity . Extending this further, suppose that the breakdown position maintains an average mean location because the generated vorticity is balanced by the vorticity being convected downstream for some given set of fixed conditions (i.e. sweep and α) as suggested by Lee and Ho [25]. The flow conditions are then in some way altered, so as to add more vorticity upstream of the breakdown without a corresponding increase in the convection rate downstream. If the breakdown is seen to move upstream, this would indicate some critical condition based on a maximum vorticity distribution may exist above which the initial vortex structure will transition to the post breakdown state. An increase in α or a decrease in sweep angle would also then imply that, momentarily, the relative vorticity generation rate becomes higher than the convective rate and the transition/breakdown point changes until a stable situation is again reached.

The distribution of vorticity throughout the vortex was therefore examined for possible maximum amounts of vorticity per unit area or volume at a chordwise location.The integration of discrete data has the effect of smoothing errors associated with the data. In order to evaluate the reliability of differentiating the discrete velocity field, the circulation, Γ, was also calculated and compared to the integration of the vorticity field over the area normal to it:

$$\Gamma = \int_{r} V \cdot dr = \int_{A} (\nabla \times V) \cdot dA = \int_{A} \Omega_x \, dA$$

The vorticity field distribution was spatially integrated and is presented with the equivalent line integral of the velocity field, for the $\Lambda = 75°$, $\alpha = 20°$ case, in Figure 7. The values are plotted outward from the core center (r = 0) where the radial distance has been nondimensionalized by the local semispan. Each curve represents a chordwise location and the circulation is seen to grow in a chordwise manner. This is what one would expect, as the feeding sheet is continually being wrapped into the vortex. The circulation and integrated vorticity values are seen to correspond quite well, which would indicate that differentiating the velocity fields does not increase the error substantially.

T ulation val s were then scaled by the local s , s*, and plotted in Figure 8. It appears that

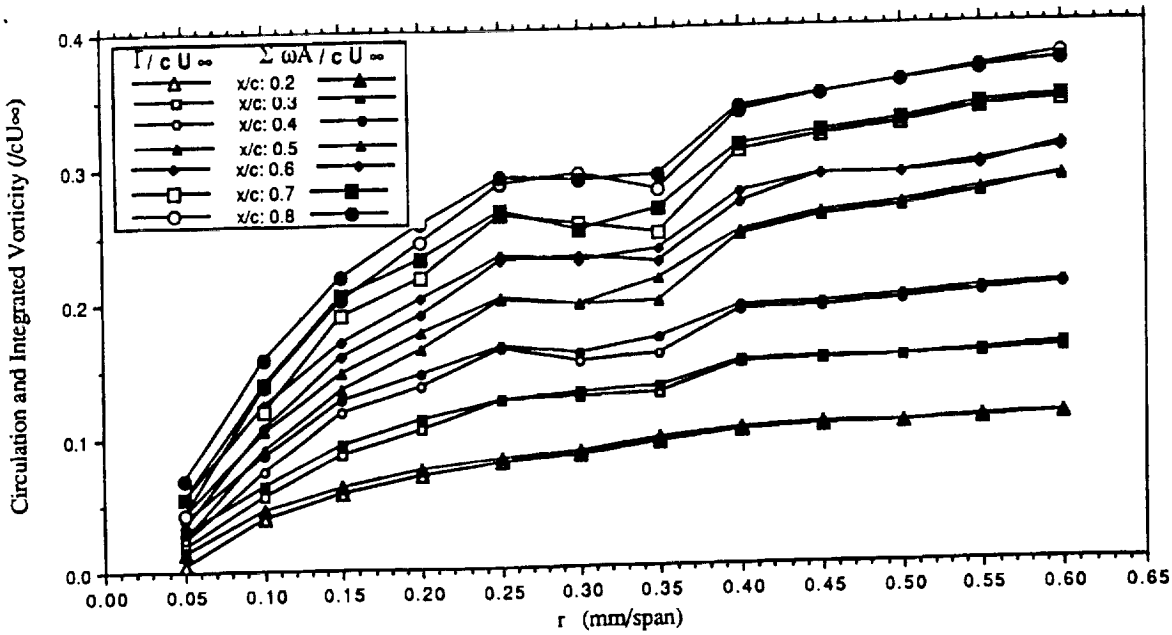

Figure 7. Radial Distribution of Circulation and Integrated Vorticity, Sweep = 75°, Angle of Attack = 20°

this has the effect of causing the curves to fall quite closely onto each other. The data taken for $\Lambda = 75°$, $\alpha = 30°$ is also shown for comparison. If scaled by the chord, $\alpha = 30°$ has a distribution similar to that of $\alpha = 20°$ in Figure 7. The data in Figure 8 would seem to imply that the chordwise development of circulation at a constant angle of attack grows in a linear manner, indicative of a conical type of flowfield.

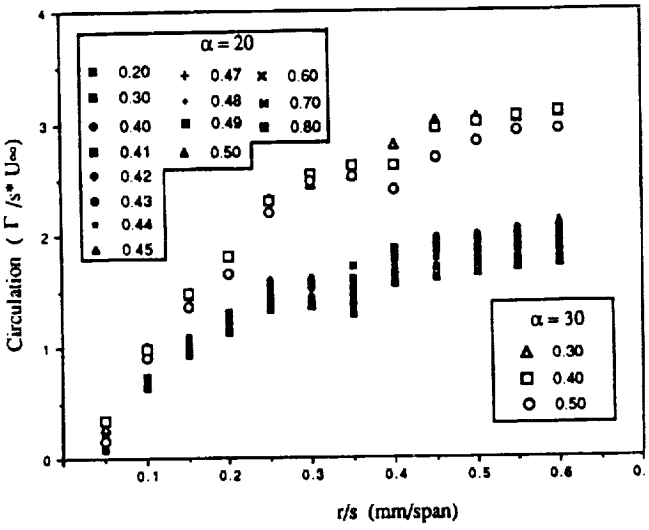

Figure 8. The Effect of Angle of Attack on the Radial Circulation Distribution Nondimensionalized by Local Semispan for Sweep = 75°

A possible way to account for the angle of attack effect would be to further incorporate some function of α as a scaling parameter. If the circulation values are divided through by, say, $\sin(\alpha)$ the results in Figure 9 are obtained. The data for $\Lambda = 70°$, $\alpha = 20°$ has also been added for comparison.

Each of the curves shown previously in Figure 7 illustrates the distribution of the circulation in the radial direction. Each curve is seen to increase to an r/s of approximately 0.25, which represents the extent of the primary vortex. A further increase in the curve profile is also observed corresponding to the

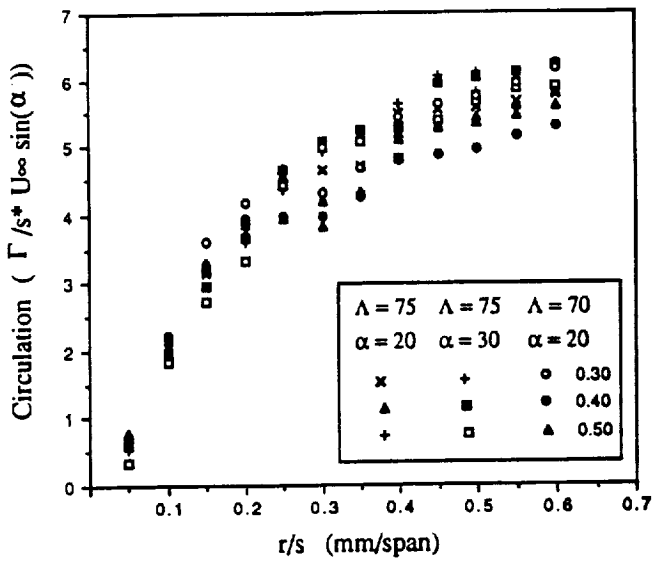

Figure 9. Radial Circulation Distribution Nondimensionalized by Local Semispan and Angle of Attack

shear layer of fluid which has separated from the leading edge. If the maximum value of the circulation scaled by the chord is plotted for each chord station, the curve shown in Figure 10a results. Although the data corresponding to the maximum radius of integration, r/s = 0.6, appears to be following a somewhat linear trend, there is widespread scatter in the data. Since the core is located at a z/s of about 0.37 to 0.40, the lower integration path is bounded by the upper surface of the wing for any r/s values greater than this. Depending on the proximity of the probe to the wing surface, velocity components contributing to a negative vorticity component will have a varied effect on the resulting integration. A better representation is obtained if the circulation values corresponding to the initial leveling off of the curves in Figure 7 is used. The values for this radial distance of r/s = 0.25 are also plotted in Figure 10a. A much smaller scatter is present in the data. The

values tend to follow a near linear distribution, exce[illegible] near the aft of the wing surface, whereupon a le[illegible]ling off is observed.

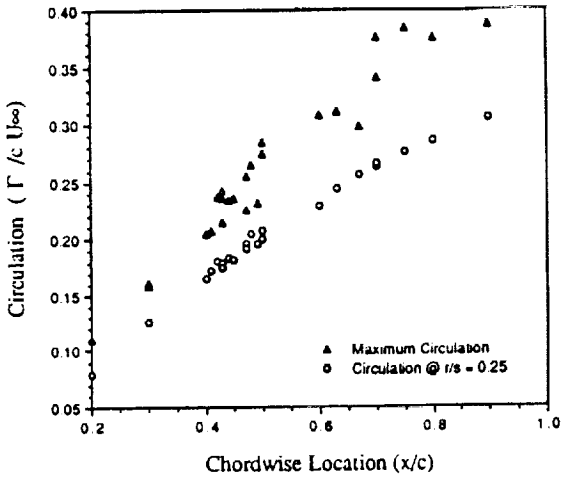

(a)

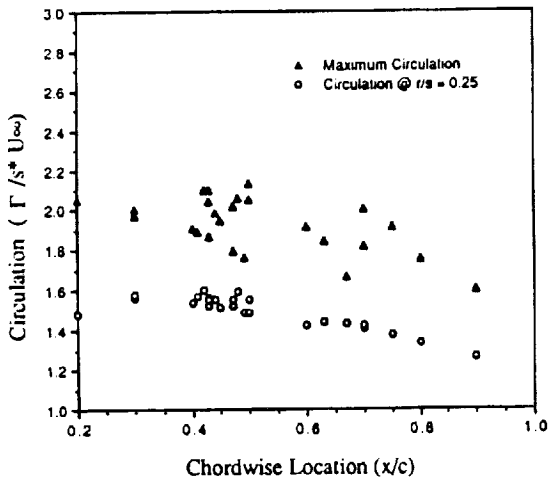

(b)

Figure 10. Chordwise Comparison of Circulation for sweep = 75°, Angle of Attack = 20°, nondimensionalized using a) chord, b) local semispan.

Scaling the values in Figure 10a by s* instead of c produces the distributions of Figure 10b. Both the r/s = 0.6 and r/s = 0.25 cases indicate values which are dropping slightly in the axial direction. The scatter in the maximum values appears to be even greater than in Figure 10a. It should be remembered however, than nondimensionalization of data can introduce other subtleties. The chord used to scale the data is a constant for all the cases presented here and simply multiplies the data by approximately 2.5, while maintaining the same relative distance between curves. On the otherhand, if the values in Figure 10a are multiplied by c/s* in order to scale by the local semispan, that is equivalent to multiplying by tan (Λ) / (x/c). In effect, any differences are magnified (local chord)$^{-1}$.

The data from the other wing configurations is presented in Figure 11a, along with that of Figure 10, for r/s = 0.25 . For the 75 degree sweep case, the circulation [illegible] 30° angle of attack case is seen to be greater than α = 20, as one would expect. The Λ = [illegible], α = 20° case is also seen to lie above the data of Figure 10, indicating the vortex over the 70° sweep wing to be stronger than that of 75° for the same angle of attack. This is in accordance with the idea that a stronger vortex causes breakdown to occur sooner; that is, sweeping a wing forward at a constant angle of attack causes breakdown to occur closer to the apex due to increased vortex strength. An interesting observation is made of the data if s* is again used as the scaling parameter in Figure 11b. The data for Λ = 70° is seen to fall below that of Λ = 75° for α = 20°.This would seem to imply that there is a lower total amount of distributed vorticity over the 70° wing per unit span than the 75° wing, even though the absolute values are larger. The spanwise distribution of vorticity will be examined in more detail using core traverse data later in this paper.

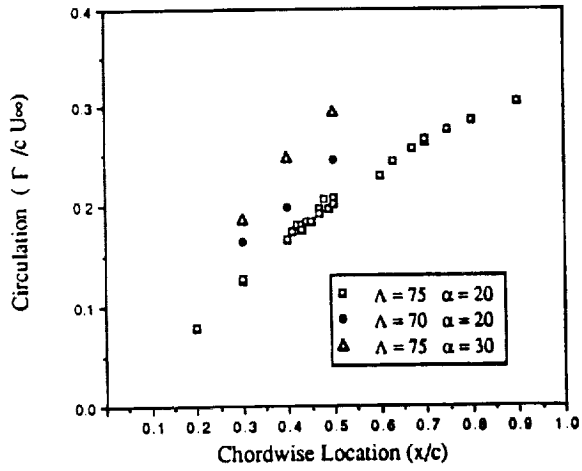

(a)

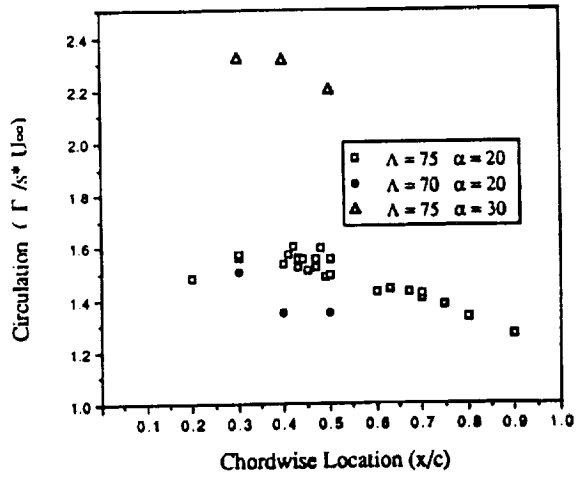

(b)

Figure 11. The Effect of Angle of Attack and Sweep on the Chordwise Circulation Distribution at r/s = 0.25 Nondimensionalized using a) chord, b) local semispan.

The close agreement of the integrated vorticity with the circulation can be exploited to examine the separate changes in the total positive and total negative vorticity which is not evident from the circulation alone. Integrating the positive and negative values of vorticity separately over their respective areas leads to the results shown in Figure 12. From Figure 12a, it appears that the amount of negative vorticity present above the wing is relatively similar for all three configurations, the Λ = 70°, α = 20° case

having the largest magnitude at each respective chord location. The positive values, however, show a marked difference. The 70° swept wing at 20° angle of attack is seen to approach the values associated with the 75° sweep at an angle of attack of 30°. Scaling by s* causes the positively integrated values to remain relatively constant or slightly decrease with increasing chord location. In addition, the $\Lambda = 70°$, $\alpha = 20°$ case is seen to fall in the same region as $\Lambda = 75°$, $\alpha = 20°$. The negative vorticity values remain together at approximately a constant value for all three cases.

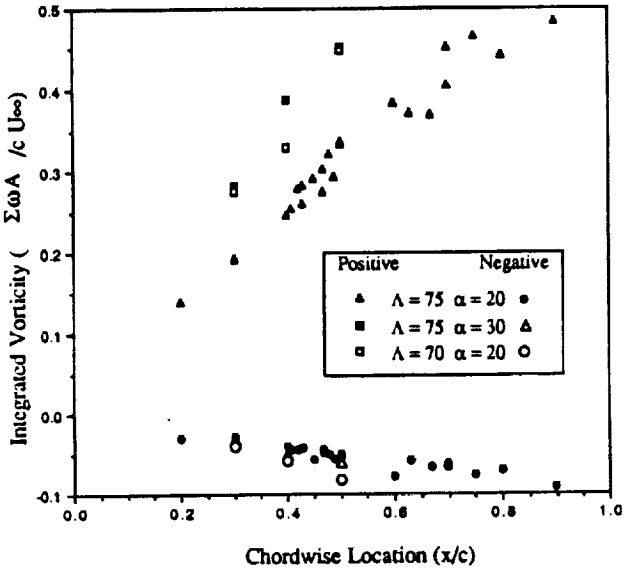

(a)

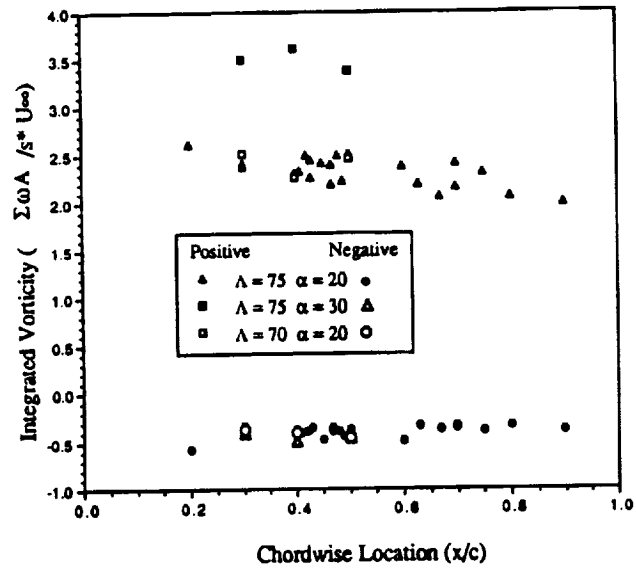

(b)

Figure 12. Chordwise Variation of Integrated Vorticity Nondimensionalized using a) chord, b) local semispan.

A similarity relationship proposed by Hemsch and Luckring [34] for the vortex circulation as a function of the apex half angle, ε, angle of attack, chord and freestream velocity. It has the form:

$$g = \frac{\Gamma}{U_\infty c \tan^2\varepsilon \cos\alpha} = AK^n \quad \text{where } K = \frac{\tan\alpha}{\tan\varepsilon}$$

for some value n. Hemsch and Luckring found that if g and K are plotted in a log-log format, a fit of the

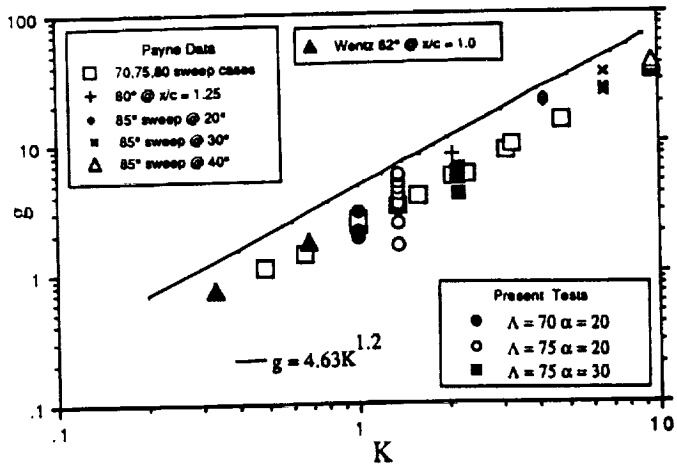

(a)

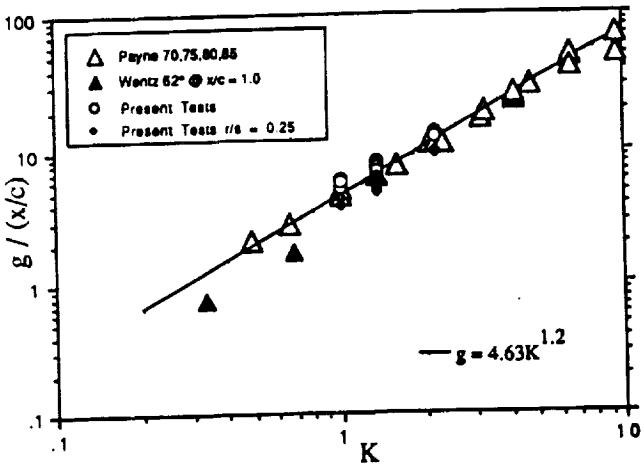

(b)

Figure 13. Correlation of Hemsch and Luckring a) g vs K, b) g/(x/c) vs K

form $g = AK^{1.2}$ was seen for data obtained from Wentz and MacMahon [35], $\Lambda = 62°$ and Delery, Pagan, and Solignac [36], ranging from g of 0.5 to 10.0 and K of 0.2 to 2.0. Theory by Smith [37] resulted in the form $g = 4.63K^n$. For comparison, seven hole probe data from Payne [4,33] is plotted in Figure 13a with that of Wentz and MacMahon and the curve of Smith for n = 1.2. Payne's data represents sweep angles of 70°, 75°, 80°, and 85° at various chord locations. It is seen to follow the line of Smith to a g of 100 and a K of 10.

The data from this investigation, representing three K values, was also plotted in Figure 13a and the expected collapse of data was not immediately evident. Hemsch and Luckring used data that was acquired in the wake of the models. Since the present tests were conducted at locations above the wing surface, a further scaling of g by the local chord ratio, x/c, was found to bring the data into line with that of Smith as shown in Figure 13b. This same scaling was used on the data of Payne and is shown in Figure 13b also. Manipulation of the above expression of Hemsch and Luckring to include the ratio x/c and expressing it in terms of s* leads to the following:

$$g = \frac{\Gamma}{U_\infty s^* \tan\varepsilon \cos\alpha}$$

If g is further divided through by K:

$$g = \frac{\Gamma(\tan\varepsilon \cos\alpha)^{n-1}}{U_\infty s^* (\sin\alpha)^n}$$

or

$$g = \frac{\Gamma(\tan\varepsilon \cos\alpha)^{0.2}}{U_\infty s^* (\sin\alpha)^{1.2}} \qquad \text{for } n = 1.2$$

where g is now simply equal to a constant. It is interesting to see how closely this corresponds to the function used in Figure 9 and that if n = 1, they would be exactly identical.

The characterization of the circulation shown above leads to an overall view of the flowfield for each wing configuration and is helpful in evaluating gross properties, such as the lift, at a particular set of test conditions. Unfortunately, the mechanism for the breakdown process is not elucidated and a more detailed look at the chordwise vorticity distributions was undertaken. In an effort to examine the validity of the theoretical ideas proposed by Brown and Lopez [22] as well as investigate what appears to be unexpected spanwise vorticity density results of Figure 11b above, values of Ω_ϕ and Ω_X were calculated based on the grid traverse through the core center utilizing polar coordinates. Under the assumption that the radial velocity and its gradient were negligible compared to the other terms along the traverse through the core:

$$\Omega_\phi = -\frac{\partial V_x}{\partial r} = -\frac{\partial u}{\partial r}$$

and

$$\Omega_X = \frac{V_\phi}{r} + \frac{\partial V_\phi}{\partial r} = \frac{w}{r} + \frac{\partial w}{\partial r}$$

The velocities based on the traverse through the core, and corresponding to the $\Lambda = 75°$, $\alpha = 20°$, x/c = 0.50 data in Figure 5, are plotted in Figure 14a against distance from the core center. The z/s location for the traverse was based on the maximum value of u/U_∞. As can be seen, the radial velocity, $v = V_r$ along the traverse can be regarded as negligible compared to the respective values of u and w, or V_X and V_ϕ. The nondimensional calculated values of Ω_X and Ω_ϕ are given in Figures 14b and 14c. The axial vorticity is seen to increase to a maximum at the center of the core. The earlier maximum, presented in Figure 6b, based on the spatial derivative in Cartesian coordinates shows a comparable value. In a similar manner, Ω_ϕ also increases as it nears the core centerline, however it drops to a value of zero at r/s = 0. Since $\partial u/dr$ is always negative with increasing distance from the core, as indicated in Figure 14a, Ω_ϕ is always positive except at r/s = 0 where u is a maximum and the gradient becomes zero.

The majority of the axial vorticity component appears to be confined to 10% of the span on either side of the core center location, r/s = ±0.1. A slight rise also occurs at r/s = 0.30, probably due to the shear layer in the feeding sheet. The azimuthal vorticity is seen to have a wider, more erratic distribution. It also appears to have a rise at r/s = 0.30 due to the feeding sheet.

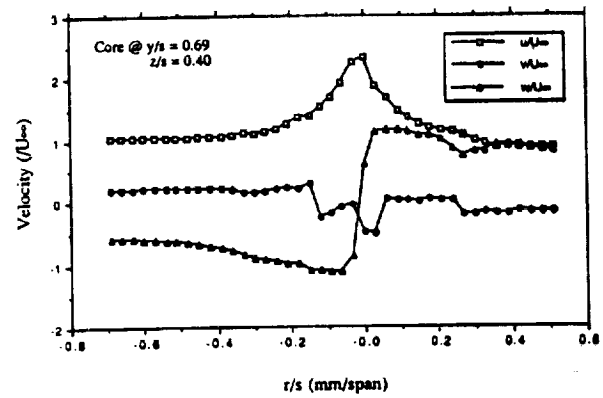

(a)

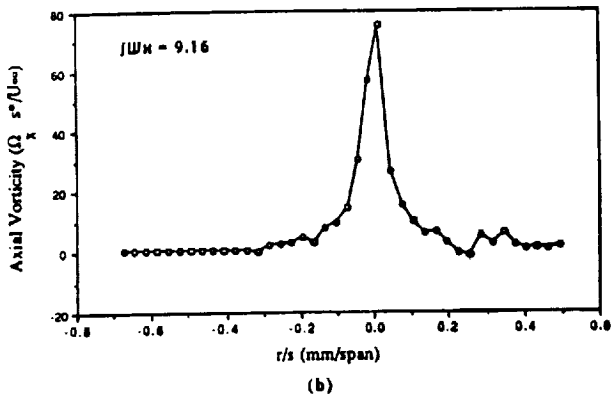

(b)

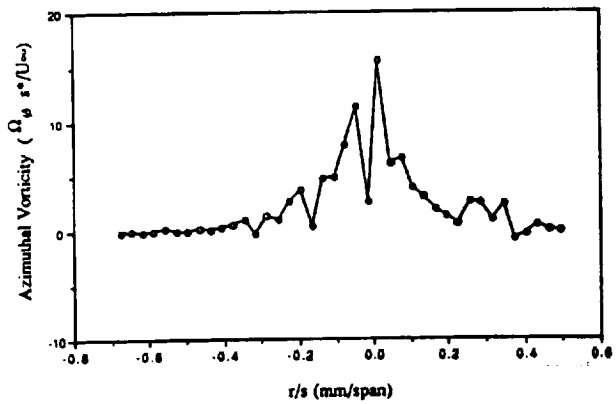

(c)

Figure 14. Core Flowfield Profiles for Sweep = 75°, Angle of Attack = 20°, x/c = 0.50 a) Velocity Components, b) Axial Vorticity, Ωx, c) Azimuthal Vorticity, Ωφ

If the axial vorticity profiles are now overlaid for each of the measured x/c locations, Figure 15a, similar profiles are seen to exist at each station. In light of the fact that no breakdown is occurring over the wing, this would seem to be acceptable. Both $\Lambda = 75°$, $\alpha = 30°$ and $\Lambda = 70°$, $\alpha = 20°$ exhibited similar features. It was hoped that some indication of the imminent breakdown, especially with the $\Lambda = 75°$, $\alpha = 30°$ case, would be evident from these distributions. This premise was based on results derived using an

earlier investigators' velocity data. Axial vorticity was calculated from LDA velocity data acquired by Iwanski [38] over a one inch thick, 70° sweep, flat plate delta at $\alpha = 30°$. The different chord stations are presented in Figure 15b. The axial vorticity profile distribution is seen to increase in magnitude and narrow in width in the downstream direction, up to x/c = .411. The peak then broadens and a reduction in the values is seen further downstream as the breakdown region is entered.

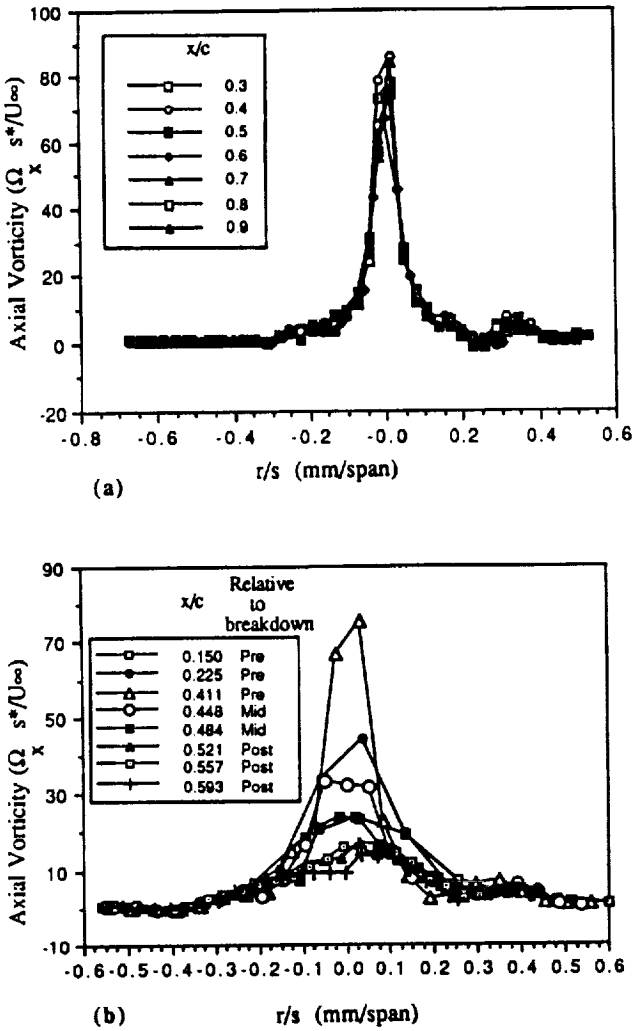

Figure 15. Axial Vorticity Distributions a) Present Tests b)Iwanski data

These calculated axial vorticity values of Iwanski were then nondimensionally integrated along each respective semispan to derive a set of values indicative of the local vorticity density distribution which are plotted against their chord locations in Figure 16a. Also included are the values of the axial component of helicity, obtained by taking the dot product of the vorticity field with the velocity field. Both the integrated vorticity and the helicity components appear to reach a maximum at a distance of about 10 to 15% of the chord upstream of the breakdown region. Whether this indicates that the vortex reaches a saturated or critical condition is still open to question, due to the scarcity of data. This is then followed by a rapid decline through the breakdown region and beyond. Figure 16b depicts the integrated results for the present tests. No trend is seen for $\Lambda = 75°$, $\alpha = 20°$. The data for the $\Lambda = 75°$, $\alpha = 30°$ configuration does not give any indication of the upcoming flow transition, however the probe was still upstream of breakdown and the x/c increment was not nearly as fine as that used by Iwanski.

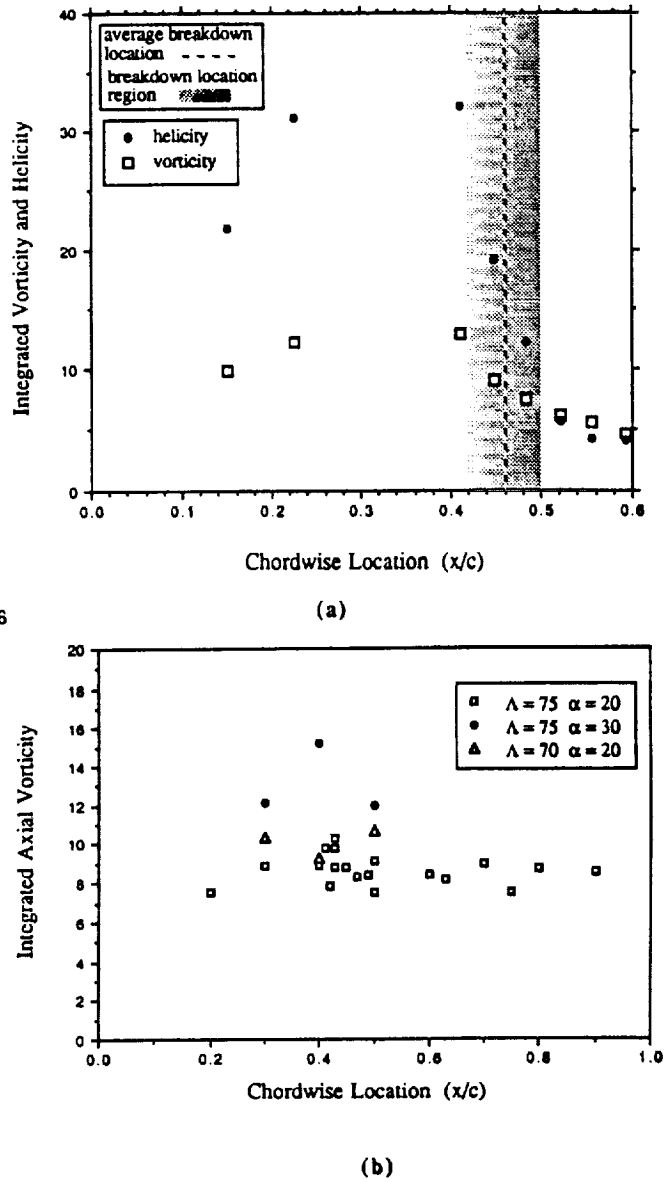

Figure 16. Chordwise Distributions of Integrated Properties Nondimensioned by the Local Semispan a)Iwanski data, b) Present Tests

Azimuthal vorticity values derived from Iwanski's data are presented in Figure 17a. This component of vorticity becomes negative at certain spanwise locations as soon as the breakdown region is entered, supporting the ideas of Brown and Lopez [22]. The azimuthal component appears to reach a maximum negative value, however as this data represents time averaged values of a highly fluctuating region, care should be taken when drawing conclusions. It should be noted that there may be a non-negligible radial velocity component in the expansion region of the breakdown region, which would act to provide a positive contribution to Ω_ϕ, which is not considered in the evaluation of Iwanski's data due to a lack of sufficient information. Pagan and Solignac [30] also determined that the value of Ω_ϕ becomes negative as the breakdown region is encountered. Their spatial results indicate local minimums shortly after the

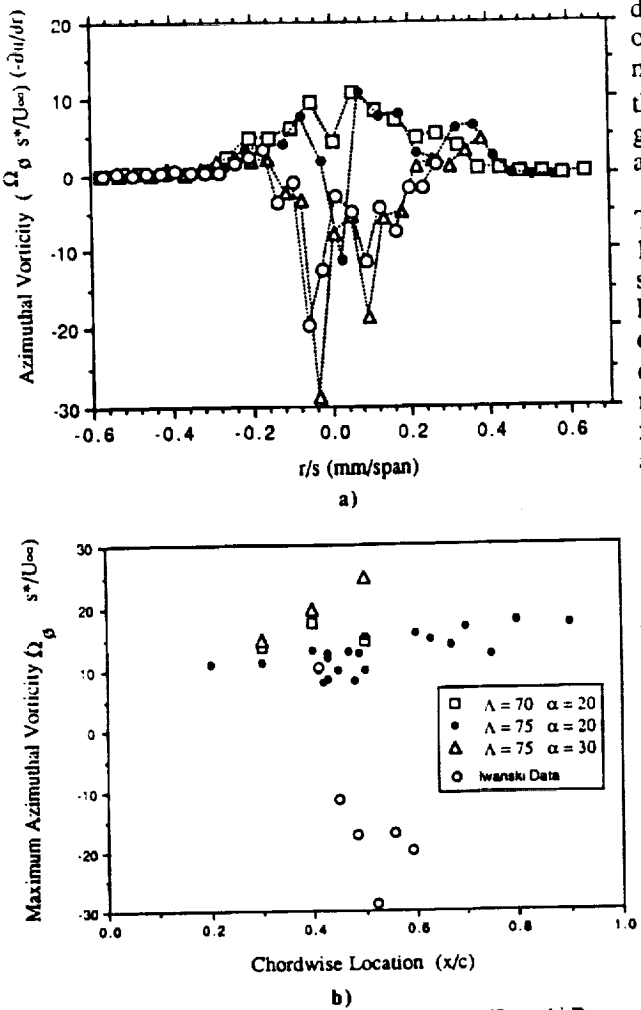

Figure 17. Azimuthal vorticity Distributions a)Iwanski Data b) Maximum Azimuthal Vorticity

breakdown. They conclude that the vorticity vector, Ω, rotates from an essentially longitudinal direction to a generally tangential one in the breakdown zone as Brown and Lopez's analytical hypothesis surmise.

Since there is no sense physically in integrating the azimuthal vorticity distributions, the maximum values of Ω_ϕ were plotted instead in Figure 17b. These values represent the maximum gradient of the axial velocity and are increasing slightly in the axial direction for the present tests. The data of Iwanski reflects the change from a positive to a negative sense. It should be noted that unless there is a local axial velocity deficit, -∂u/dr will always be positive. Other investigators have shown this to occur in the breakdown region, but the present method was found to be inaccurate for regions of the flow where u is much less than v or w and the low axial velocity regions present at breakdown gave results which could not be considered reliable. In addition negative values of u could not be measured using this method.

Flow visualization at the University of Notre Dame has indicated an additionally interesting phenomena that while the outer flow region of the vortex seems to scale with the local geometry of the wing, the subcore appears to maintain a more or less constant diameter.The nature of the data in Figure 14 leads to the possibility of two core size definitions: a jet effect core due to the presence of the axial velocity component and a much smaller core based on the distance between the maximum and minimum values of w or V_ϕ, usually referred to as the subcore. If a minimum value of u/U_∞, say 1.5, is used to set a threshold cutoff, a jet core can be defined and the growth rate compared to that of the subcore defined above.

The evaluated core diameters are presented in Figure 18, both in absolute units and scaled by the local semispan of the wing. The grid resolution of 0.03 y/s leads to more scatter in the determination of the size of the subcore than the jet core, however Figure 18a does indicate that the jet core is growing at a faster rate than the subcore, albeit both are in a linear fashion. Scaling by the semispan shows that both cores are scaling by the local geometry. Closer inspection, though, reveals that the jet core may appear to be slightly shrinking in size relative to the local span and that the subcore is growing. These could be the effects of diffusion acting on the subcore region and/ or the jet. Two finer grid resolution (0.015 y/s) stations are also included in Figure 18 and would seem to indicate a more constant core diameter on the absolute scale. The scatter of the data makes interpretation difficult and more data will be required at a finer grid resolution before any definitive statements can be made.

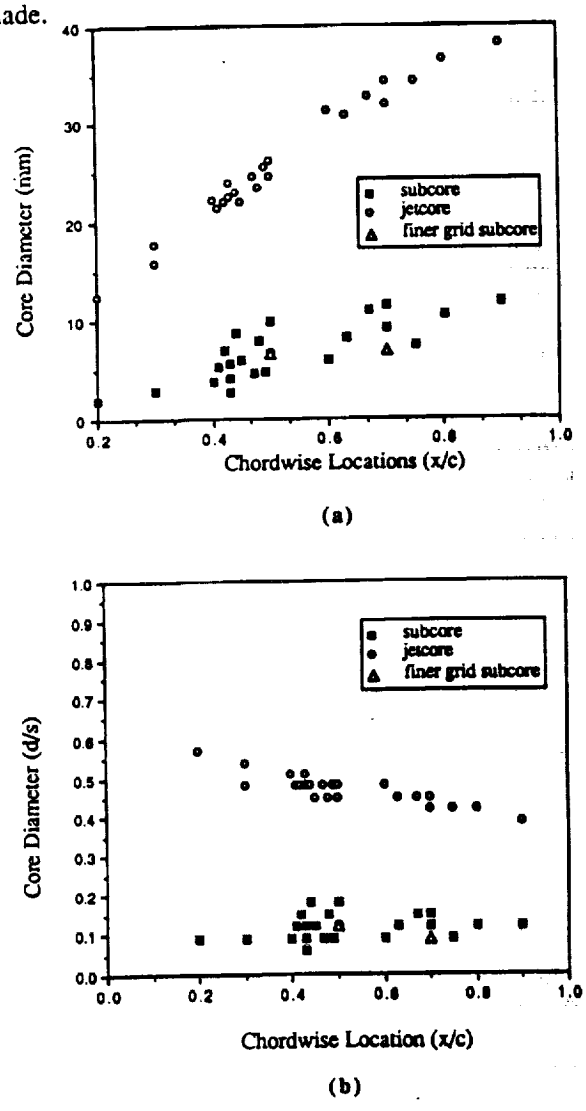

Figure 18. Jet core and Subcore Diametersa) millimetres, and b) scaled by local span

Other investigators have also looked into this aspect of the subcore growth. Verhaagen and van Ransbeeck [28] have measured a more or less constant subcore diameter from x/c = 0.1 to 0.7 on a 2.22 m, 76° swept delta wing, indicating a cylindrical rather than conical flow. Data obtained from Hawk, Barnett, and O'Neil [39], however, points to a linear type of core growth with chordwise distance over a 762 mm chord, 70° swept wing. These discrepancies again indicate that due to such factors as grid resolution, which is usually not compared between experimental data sets, differing statements concerning observable properties can exist between investigators and comparisons should be examined in light of these factors.

Conclusions

Scaling of the radial circulation distribution or the vorticity by the local semispan indicates the distributions to be similar at each chordwise location for regions of pre-breakdown vortex flow. This is a good indication that the local semispan is a variable which should be incorporated into any nondimensionalization scheme used to examine flows generated by swept leading edge geometries. This is further substantiated by the results obtained using the correlation of Hemsch and Luckring. Incorporating the factor x/c appears to correlate circulation distributions in regions where the vortex size and strength are increasing, such as over a delta wing. The circulation at a given radius from the core center is also seen to grow in a nearly linear fashion in the chordwise direction.

Spanwise vorticity distributions based on a single traverse through the core of the vortex also scale with the local geometry in the pre-breakdown state. The vorticity distribution is severely altered as the breakdown region is encountered and appears to indicate there is some maximum type of vorticity distribution that may occur in the region just preceding breakdown. The maximum azimuthal vorticity also maintains a more or less constant value in the vortex upstream of breakdown, but is observed to become negative upon entering the breakdown zone.

The majority of the axial vorticity appears to be confined to the subcore region of the vortex, at least with respect to the pre-breakdown vortex state. The use of the maximum value of axial vorticity can be deceptive, however, in determining the local strength of the vortex structure. Factors such as grid resolution should be accounted for when comparisons of data are made.

The distributions of negative axial vorticity are similar for the different configurations investigated here, despite geometric and angle of attack differences. Adjustment of the flowfield to changing test conditions seems to occur for the most part in the positive axial vorticity regions. Whether this indicates that the secondary vortex structure is a relatively constant influence or perhaps solely a function of the Reynolds number remains to be seen.

The jet core and subcore growth rates both appear to be functions of the local semispan, although they are growing at different rates. Relative to the local geometry, the subcore appears to be constant and the jet core shrinking in size in the axial direction. Finer grid data and flow visualization indicate that the subcore decreases in size relative to the local geometry; that is, it maintains a constant diameter.

Acknowledgements

The authors gratefully acknowledge the support of the NASA Langley Research Center, grant NAG-1-1156, and the University of Notre Dame for this research effort. In addition they wish to thank Isabelle Maillot and Florence Pipelier of the B.R.I. École Polytechnique Féminine for their computational assistance.

References

[1] Lambourne, N. C., and Bryer, D. W., "The Bursting of Leading Edge Vortices-Some Observations and Discussion of the Phenomena," Aeronautical Research Council, Reports and Memoranda, No. 3282, April 1961.

[2] Harvey, J. K., "Some Observations of the Vortex Breakdown Phenomenon" Journal of Fluid Mechanics Vol. 14 pp. 585-592, 1962.

[3] Erickson, Gary E., "Vortex Flow Correlation",Technical Report AFWAL-TR-80-3143 Flight Dynamics Laboratory, Wright Patterson Air Force Base, January 1981.

[4] Payne, F. M. "The Structure of Leading Edge Vortex Flows Including Vortex Breakdown" PhD Dissertation, University of Notre Dame, May 1987.

[5] Kegelman, J.T. and Roos, F.W. "Effects of Leading Edge shape and Vortex Burst on the Flowfield of a 70-Degree-Sweep Delta Wing" AIAA Paper 89-0086 Jan 9-12, 1989 Reno, NA.

[6] Wentz, W.H. and Kohlman D.L. "Vortex Breakdown on Slender Sharp Edged Wings." Journal of Aircraft Vol.8 #3. March 1971 (AIAA Paper 69-778 July 14-16, 1969).

[7] Wentz, W.H. and Kohlman D.L. "Wind Tunnel Investigations of Vortex Breakdown on Slender Sharp Edged Wings" NASA CR-98737, 1969.

[8] Wedemeyer, E. "Vortex Breakdown", No.9, AGARD-LS-121, December 1982.

[9] Jones, J.P. "The breakdown of vortices in separated flow", Dept of Aer and Astro, Unv. of Southhampton, Rep. No. 140, 1960.

[10] Squire, H.B. Imperial College, London, Dep. of Aero. Report. No. 102, 1960.

[11] Ludweig, H. "Contribution to the Explanation of the Instability of Vortex Cores Above Lifting Delta Wings", Aero. Versuchsanstalt, Gottingen, Rep. AVA/61 A01, 1961.

[12] Randall, J.D. and Leibovich, S., "The Critical State: A Trapped Wave Model of Vortex Breakdown", J. Fluid Mech., Vol.58, 1973.

[13] Benjamin, T.B. "Theory of Vortex Breakdown Phenomena" J. Fluid Mech., Vol.14, June 1962.

[14] Escudier, M.P. and Keller J.J. "Vortex Breakdown: A Two Stage Transition" AGARD-CP-342, No. 25, April 1983.

[15] Gartshore, I. S., "Recent Work In Swirling Incompressible Flow", NRL (Canada), LR-343, June 1962.

[16] Hall, M.G. " The Structure of Concentrated Vortex Cores",Progress in Aeronautical Science(Ed. D. Kucheman), Vol 7, 1966.

[17] Bossel, H.H. "Vortex Breakdown Flowfield", Phys. of Fluids, Vol. 12, No. 3, March 1969.

[18] Mager, A. "Dissipation and Breakdown of a Wingtip Vortex" J. Fluid Mech., Vol.55 1972.

[19] Wilson, J.D. "Calculations of Vortex Breakdown Locations for Flow Over Delta Wings", J.Aircraft, Vol. 145, No. 10, Oct 1977.

[20] Grabowski, W.J. and Berger, S.A."Solutions of the Navier Stokes Equations for Vortex Breakdown." J. Fluid Mech., Vol.75, 1976.

[21] Hall, M.G. " Vortex Breakdown", Ann. Review of Fluid Mech., Vol. 4, 1972.

[22] Brown, G.L. and Lopez, J.M. "Axisymmetric Vortex Breakdown Part II: Physical Mechanisms" Aeronautical Research Laboratories, P.O. Box 4331, Melbourne, Vic., 3001, Australia. A.R.L Aero. Rep. 173, AR-004-572 (1988).

[23] O'Neil, P.J., Barnett, R.M., and Louie, C.M., "Numerical Simulation of Leading Edge Vortex Breakdown Using an Euler Code" 89-2189-CP.

[24] Ekaterinaris, J. and Schiff, L.B., "Vortical Flows over Delta Wings and Numerical Prediction of Vortex Breakdown" AIAA 90-0102 January 8-11, 1990 Reno, Nevada.

[25] Lee, M. and Ho, C-M. " 'Vortex Dynamics of Delta Wings' Frontiers in Experimental Fluid Mechanics" Lecture Notes in Engineering Vol. 46 © 1989 Springer-Verlag, Berlin.

[26] Visser, K.D., Nelson, R.C., and Ng, T.T., "Method of Cold Smoke Generation for Vortex Core Tagging" AIAA Journal of Aircraft Vol.25, No.11 November 1988.

[27] Kjelgaard, S.O. and Sellers, W.L. III, "Detailed Flowfield Measurements over a 75° Swept Delta Wing for Code Validation" AGARD Symposium on Validation of Computational Fluid Dynamics, Lisbon, Portugal, May 2-5, 1988.

[28] Verhaagen, N. and van Ransbeeck, P. "Experimental and Numerical Investigation of the Flow in the Core of the Leading Edge Vortex" 28th AIAA Aerospace Scences Meeting, AIAA 90-0384 January 8-11, 1990 Reno, Nevada.

[29] Carcaillet, R., Manie, F., Pagan, D. and Solignac, J.L. "Leading Edge Vortex Flow Over a 75 Degree-Sweep Delta Wing- Experimental and Computational Results." ICAS 86.

[30] Pagan, D. and Solignac, J.L. "Experimental Study of the Breakdown of a Vortex Generated By a Delta Wing" La Recherche Aérospatiale, No 3, May-June 1986.

[31] Sherif, S.A. and Pletcher, R.H. " A Normal-Sensor Hot Wire/Film Probe Method for the Analysis of Highly Three Dimensional Flows" ASME Applied Mechanics Biomechanical and Fluid Engineering FED Vol 49, p19-22, Cinncinati, OH, 1987

[32] Jørgensen, F.E. "Directional Sensitivity of Wire and Fiber-film Probes *An Experimental Study*" DISA Information No.11 May 1971.

[33] Payne, F.M., Ng, T.T.,, and Nelson, R.C. "Experimental Study of the Velocity field on a Delta Wing" 19th AIAA Fluid Dynamics, Plasma Dynamics, and Laser Conference, AIAA-87-1231, Honolulu, Hawaii, June 8-10, 1987.

[34] Hemsch, M. J. and Luckring, J. M. "Connection between Leading Edge Sweep, Vortex Lift and Vortex Strength for Delta Wings" AIAA Journal of Aircraft Vol.27, No.5 May 1990.

[35] Wentz, W.H. and MacMahon, M.C., "Further Experimental Investigations of Delta and Double Delta Flowfields at Low Speeds", NASA CR-714, Feb 1967.

[36] Delery, J., Pagan, D. and Solignac, J.L., "On the Breakdown of the Vortex Induced by a Delta Wing" Colloquium on Vortex Control and Breakdown Behavior, Baden, Switzerland, ONERA TP 1987-105, April 6-7, 1987.

[37] Smith, J.H.B. "Calculations of the Flow over Thick, Conical, Slender Wings with Leading Edge Separation" ARC R&M 3694, March 1971

[38] Iwanski, Kenneth P. "An Investigation of the Vortex Flow Over a Delta Wing with and without External Jet Blowing" Masters Thesis, University of Notre Dame, April 1988.

[39] Hawk, J., Barnett, R., and O'Neil, P. "Investigation of High Angle of Attack Vortical Flow Over Delta Wings" 28th AIAA Aerospace Scences Meeting, AIAA 90-0101 January 8-11, 1990 Reno, Nevada.